Modifying natural droplet systems by charge injection

Letter

Modifying natural droplet systems by charge injection

R. Giles Harrison, Graeme J. Marlton,* Maarten H. P. Ambaum, and Keri A. Nicoll
Department of Meteorology, University of Reading, Reading RG6 6BB, United Kingdom

(Received 6 January 2022; accepted 5 May 2022; published 31 May 2022)

Modifying droplet behavior has wide applications, from removing pathogens to increasing rainfall. In an environmental experiment, negative charge release is demonstrated to influence a natural fog. During charge emission, the average mass concentration of 1 μm droplets increased by 95.3%. For smaller droplets, concentrations during charge emission exceeded those without charge emission at the 99% confidence level. This is consistent with charge both facilitating formation of small droplets and inhibiting their evaporation. Physics-based droplet modification has immediate relevance to weather modification and, conceivably, pathogen control, without the introduction of additional chemical materials.

DOI: 10.1103/PhysRevResearch.4.L022050

I. INTRODUCTION

Droplet systems are ubiquitous in nature, such as in clouds, or exhalations which transmit disease. In weather modification, attempts are made by chemical means to encourage small droplet growth in clouds to produce rain. Alternatives consuming less resource without generating residues are, however, desirable. One physics-based approach is to introduce charge. Charge affects droplet stability [1], inter-droplet forces [2–4], and collision efficiencies [5–7], changing the droplet size distribution. Further, charge modifies aerosol deposition, allowing targeted material delivery or decontamination [8,9]. New methods to disrupt droplet systems carrying pathogens such as COVID-19 may also have contemporary relevance [10], if a therapeutic benefit can be demonstrated.

Observations of ionization affecting water clouds [11,12] motivate experiments to investigate charge effects on natural drop systems. Although non-thunderstorm-cloud droplets are commonly charged [13], direct experimentation is difficult. Surface fogs offer a more practical alternative, having droplet sizes (1–10 μm diameter) similar to some clouds [14,15] and exhaled drops [16]. Observations of charge release into fog are described here. Relevant theory on the stability of charged droplets is given first, followed by experimental implementation. Results are then summarized and discussed.

II. THEORY

A. Formation of charged droplets

Droplets form on small aerosol particles, influenced by vapor supersaturation and charge [1,17]. The change in free energy ΔG when a water droplet of radius a forms on a cloud condensation nucleus of radius a_0 is

$$\Delta G = -\frac{4}{3}\pi a^3 \rho_w \frac{N_A}{M_r} k_B T_a \ln S + 4\pi a^2 \gamma + \frac{j^2 e^2}{8\pi \varepsilon_0}\left(\frac{1}{a} - \frac{1}{a_0}\right), \tag{1}$$

with M_r, ρ_w, and γ the relative molecular mass, density, and surface tension of liquid water, respectively; N_A is Avogadro's number; k_B Boltzmann's constant; T_a the droplet temperature; S the local water vapor saturation ratio; and je the charge carried (for j the number of elementary charges, e, carried) and ε_0 is the permittivity of free space. The saturation ratio required for droplet formation is found from the turning point of Eq. (1), as

$$S(a) = f_T f_R\left(1 - \frac{b}{a^3}\right). \tag{2}$$

In Eq. (2), f_T is the Thomson factor for surface tension; f_R is the Rayleigh factor for electrical forces; and the final term represents the effect of dissolved salt, with $b = \frac{3 i_V M_r m}{4\pi \rho_w M_s}$, i_V the Van't Hoff factor, M_s the relative molecular mass of the salt, and m the dissolved mass of salt. The Thomson and Rayleigh terms are given by

$$f_T = \exp\left(\frac{2\gamma}{\rho_w R_v T_a a}\right) \tag{3}$$

and

$$f_R = \exp\left(\frac{-j^2 e^2}{32\pi^2\, \varepsilon_0 R_v T_a a^4 \rho_w}\right), \tag{4}$$

respectively where R_v is the gas constant for water vapor, [17,18]. Figure 1(a) shows how increasing charge affects the water droplet formation, by decreasing the critical supersaturation and increasing the critical size.

*Present address: MetOffice, Fitzroy Road, Exeter, UK.

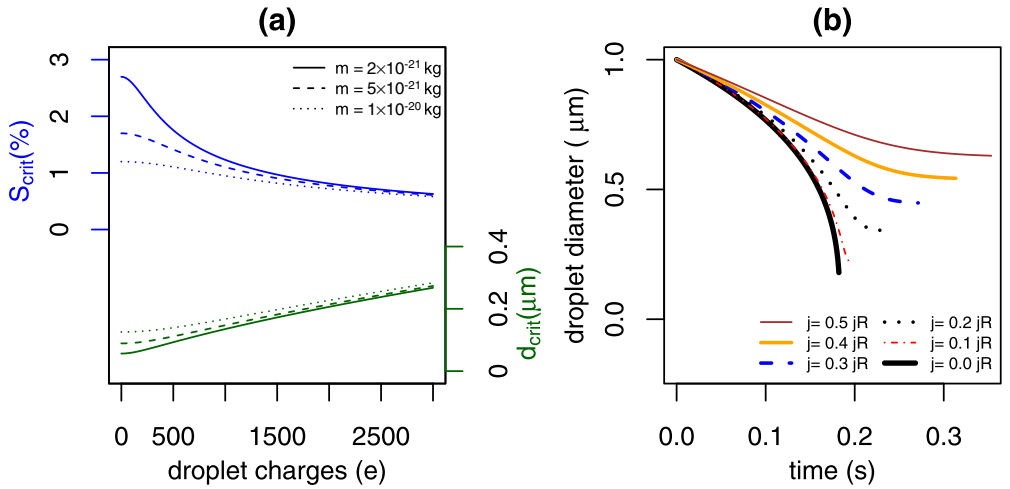

FIG. 1. (a) Droplet formation as a function of charge, showing, for a range of dissolved salt concentrations m, the critical supersaturation $S_{\rm crit}$ required (left-hand axis) and the diameter $d_{\rm crit}$ at which the droplet is stable (right-hand axis). (b) Evaporation of 1 μm diameter droplet with time, in air at 5 °C and 99.99% relative humidity, for different initial droplet charges (as a proportion of the 1 μm diameter Rayleigh limit, $j_{\rm R}$, 45246e). (Constants: $M_r = 0.018\,{\rm kg\,mol^{-1}}$, $\rho_w = 1000\,{\rm kg\,m^{-3}}$, $e = 1.6 \times 10^{-19}{\rm C}$, $\varepsilon_0 = 8.85 \times 10^{-12}\,{\rm F\,m^{-1}}$, $\gamma = 7.2 \times 10^{-2}\,{\rm N\,m^{-1}}$, $R_v = 461.5\,{\rm J\,kg^{-1}\,K^{-1}}$, $D_v = 2.91 \times 10^{-5}\,{\rm m^2\,s^{-1}}$, $k_g = 0.5918\,{\rm W\,m^{-1}\,K^{-1}}$, and $L = 2.26\,{\rm MJ\,kg^{-1}}$. $f_v = 1$ assumed).

B. Evaporation of charged droplets

Droplets evaporate according to the local vapor concentration. The variation in a droplet's radius a with time t as it evaporates is given by

$$a\frac{da}{dt} = \frac{D_v}{\rho_w R_v} f_V \left[\frac{e_\infty}{T_\infty} - f_T f_R \frac{e_s(T_a)}{T_a}\right], \tag{5}$$

for vapor diffusivity D_v, and f_V, a ventilation coefficient [15]. The difference term on the right-hand side (RHS) describes vapor transfer between the ambient environment (temperature T_∞ and vapor pressure e_∞) and a droplet with surface vapor pressure e_s. As the droplet shrinks, the Rayleigh factor f_R and Thomson factor $f_{\rm T}$ become increasingly important, with the charge effects arising through f_R. When $f_R = f_T$, a droplet of radius a is at the *Rayleigh limit* if the number of elementary charges carried is

$$j_R = 8\left(\frac{\pi\gamma\varepsilon_0 a^3}{e}\right)^{1/2}. \tag{6}$$

Alternatively, the *Rayleigh radius* can be calculated from (6) given a droplet charge [17]. If j_R is exceeded, or the droplet evaporates to become smaller than the Rayleigh radius, it will become unstable due to imbalance between electrical and surface forces [19].

Further, during evaporation, a droplet cools, with an instantaneous temperature given by Eqs. (13)–(23) of [15] as

$$T_a = T_\infty + \frac{\rho_w L}{k_g} a\frac{da}{dt}. \tag{7}$$

Here, k_g is the thermal conductivity of the surrounding gas and L the latent heat of vaporization.

Equation (5), with Eqs. (3), (4), and (7), can describe evaporation of a droplet from an initial size. Figure 1(b) shows an illustrative numerical solution for near-saturation conditions, such as in fog, using an adaptive, fourth-order Runge-Kutta method [20]. The evaporation time lengthens with increasing initial droplet charge, until the droplet reaches the Rayleigh radius when the calculation is stopped. Less charge is required to slow the evaporation if the relative humidity becomes extremely close to 100%, with a correspondingly smaller Rayleigh radius.

C. Growth by collision

Drops can grow through gravitational collisions and coalescence, although this is not expected to be important in fog due to the droplets' small collision cross sections. Nevertheless, for charged droplets, the collision efficiency $E_{\rm coll}$ increases due to electric image forces which are large and attractive at small separations, regardless of their relative polarities. For neutral drops of radii $R = 2\,\mu$m and $r = 1\,\mu$m, $E_{\rm coll} = 0.03$. This approximately doubles if both drops carry $-2e$ (elementary charges), reaching $E_{\rm coll} = 0.08$ for $-5e$ on both drops [7]. Turbulence is an additional aspect of some droplet interactions [21,22], and a fully turbulent simulation [23] indicates that the electrical effects can propagate from small droplets through to raindrops.

D. Droplet charging timescale

Establishing likely charging timescales for fogs informs the design of experiments. Charge in air is partitioned between "small ions"—molecules clustered around a core elementary ion—and aerosol or droplets, between which charge is exchanged, typically by diffusion. Atmospheric small ions produced at a volumetric rate q, with number concentrations n_+ and n_- for positive and negative ions, respectively, are governed by the ion balance equation,

$$\frac{dn_\pm}{dt} = q - \alpha n_\pm n_\mp - n_\pm \sum_{j=-\infty}^{\infty} \int_0^\infty \beta_j(a) dZ(a). \tag{8}$$

The RHS loss terms are due to ion-ion recombination and ion-droplet attachment, with coefficients α and β,

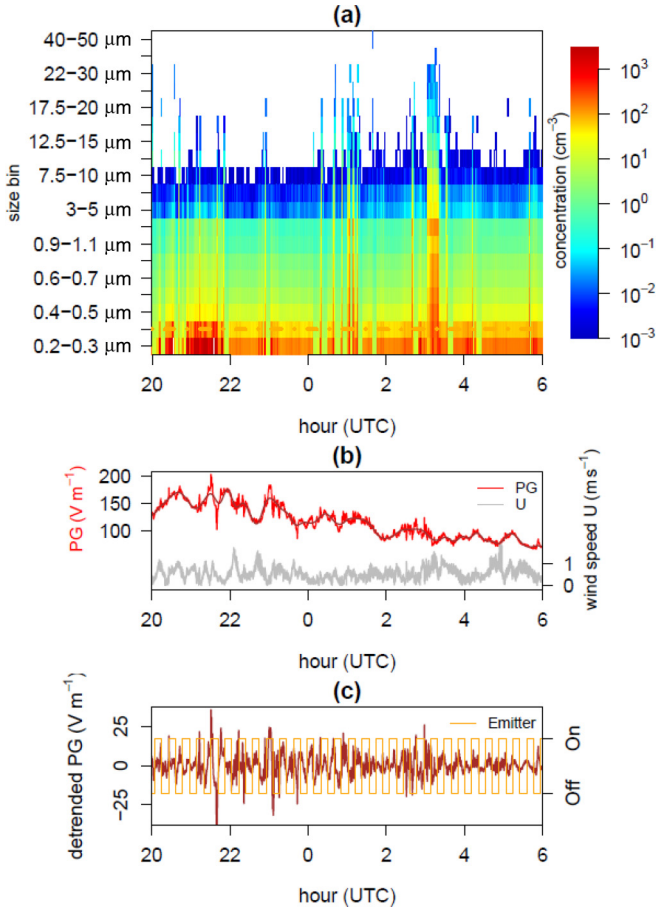

FIG. 2. Experiment time series from 20 UTC on 15 March to 06 UTC on 16 March. (a) Droplet concentrations for all size bins recorded by the LOAC. The fog threshold chosen (0.3–0.4 μm droplet concentrations in their upper quartile) is also shown, as a dashed horizontal line. (b) Potential gradient (PG) (with smoothing spline) and horizontal wind speed U at 3 m. (c) Spline-detrended PG, with emitter cycling overplotted. (U and PG were sampled at 1 s and LOAC at 1 min).

respectively. β depends on droplet size and charge [24]; hence the attachment term integrates across the droplet size spectrum, for $Z(a)$ the number concentration of droplets with radius a, with summation across all possible charges j. Simplifying to equal ion concentrations n, droplets of uniform size and concentration Z, with ion loss by attachment dominating over recombination ($n\beta Z \gg \alpha n^2$), Eq. (8) becomes

$$\frac{dn}{dt} = q - n\beta Z. \tag{9}$$

Assuming the neutral limit ($j \to 0$), an estimate for the attachment coefficient is

$$\beta_0(a) = \frac{4\pi k_B T_\infty \mu}{e} a. \tag{10}$$

For 1 μm radius droplets in a fog [14] at 278 K, with $\mu = 1.2 \times 10^{-4}$ V m^2 s^{-1} [25], $\beta_0 = 3.6 \times 10^{-11}$m^3 s^{-1}; hence with $Z = 100$ droplets cm^{-3} the ion attachment timescale $\frac{1}{\beta_0 Z}$ is 280 s.

E. Natural droplet experiment

The droplet population during charge release was examined using natural fog, in an experiment at the University of Reading's site at Sonning Farm near the River Thames (51.481 55° N, 0.897 154° W), 5 km from the campus (51.441 36° N, 0.938 07° W). Weather data showed that near-surface fogs were infrequent; hence a bespoke unattended apparatus was designed.

The fog droplet size distribution was monitored with a light optical aerosol counter (LOAC) [26], operated alongside an electric field mill, sonic anemometer, and an array of four corona emitters to inject negative charge (–0.5 nA each) into the fog (see Fig. S1 in the Supplemental Material [27]). The emitters were switched on and off every 10 min, following the timescale estimated from Eq. (10).

III. RESULTS

During spring 2020 only 3 days (of 38 operating) had thin fog, with the foggy night of 15–16 March 2020 (see Fig. S2 [27]) analyzed further. Figure 2 summarizes the experimental data, after a correction was applied for LOAC's internal real-time clock drift (see Fig. S3 [27]). In Fig. 2(a), the series of LOAC droplet size spectra is shown, illustrating the transient bursts of droplets associated with fog. From this, a threshold fog droplet concentration was derived (see also Fig. S4 [27]). Figure 2(b) shows the atmospheric electric field determined at the apparatus (n.b., plotted, by convention, as the potential gradient (PG), where for E_z, the vertical electric field, PG = $-E_z$), and the mean horizontal wind speed U. The PG increases during the more persistent fog, with wind speeds light throughout. The spline-detrended PG is shown in Fig. 2(c), on which the corona emission cycle has been overplotted.

In Fig. 3, the detrended PGs of Fig. 2(c) before [Fig. 3(a)] and during [Fig. 3(b)] the fog are compared. Before the fog formed on 15 March, the PG distributions with emitters on and off were similar, suggesting the emitted ions were being effectively dispersed away from the experimental volume. During the fog, the detrended PG distribution shifted negatively with the emitters on [Fig. 3(b)], changing from a mean of 0.5 V m^{-1} with the emitters off to –0.5 V m^{-1} with the emitters on (see also Table I). This relative PG change of ∼1% at the field mill indicates that the emitters were functioning, acting to increase negative charge in the region from which the droplets were being sampled. Nearer the emitters, the charge asymmetry is likely to be larger.

Cycling the emitters on and off allows fog droplet data to be compared, with and without additional negative ions. Droplet number concentrations in each case are compared in Fig. 4. Due to the LOAC timing correction uncertainty of ±2 min, only values from the inner 5 min of the emitters on and off periods are used, although results are similar for the inner 4 or 6 min. In Fig. 4(a), median fog droplet number concentrations during emitters on and off are shown; an increase is apparent for the smaller droplet sizes. Figure 4(b) compares the spread (as interquartile range) of the droplet concentrations for emitters on and emitters off by size, showing that the number concentration difference in Fig. 4(a) is also associated

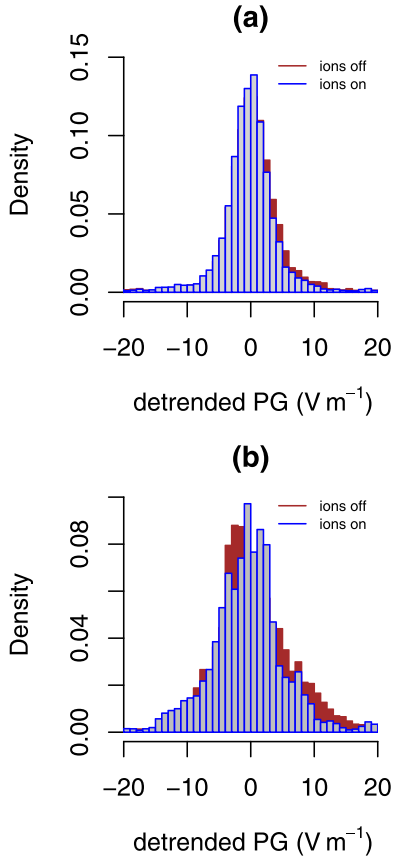

FIG. 3. Histograms of detrended potential gradient (PG) with (blue/gray bars) and without (brown solid bars) negative ion emission, during (a) 15 March up to 20 UTC and (b) for the periods with droplets exceeding the fog threshold of Fig. 2.

with increased variability during emitters on. A least squares line to the Fig. 4(b) points has a gradient of 0.86 ± 0.05 (±1 SE), significantly different from the 1:1 line around which the points would be expected to cluster if the emitter on and emitter off situations were the same. Further, statistical tests (see Fig. S5 [27]) show significant differences in droplet concentrations between the emitter on and off conditions, for the size bins between 0.3 and 1.1 μm.

Mass concentration is more physically relevant than number concentration as it reflects the distribution of liquid water. Figure 4(c) shows median mass concentrations by droplet size. The 99% confidence range on the median mass concentration during emitters off is found by bootstrapping (i.e., repeatedly computing medians from combining different subsets of the available values, and taking the inner 99%). Figure 4(c) shows that the increased mass concentration of smaller droplets up to 1.1 μm during charge emission lies beyond the range of the variability occurring naturally without charge emission (see also Fig. S5 [27]): the 1.1 μm droplets' mass concentration increases by 95.3%. Mean mass concentrations for the small sizes steadily increase during emitters on and decrease during emitters off (Fig. S6 [27]). For larger droplets ($\gg$1 μm), no significant change occurs, consistent with the Coulomb barrier inhibiting collisions [23], which is an additional contribution to stabilizing the droplet distribution.

IV. DISCUSSION

This experiment shows introduction of negative ions into an unbounded natural fog is associated with more abundant 1 μm diameter droplets. Instrument effects need to be considered as a possible cause, as droplet collection and sampling might be influenced by drop charging. A previous generation instrument to LOAC, STAC, was examined for this, and showed no difference in laboratory test measurements with and without prior charged particle removal using an electrostatic trap [28]. Further, in the Sonning experiment, charging might be expected to deposit charged droplets in the plastic inlet or laser chamber of the LOAC, reducing the measured concentrations. The opposite effect, of an increase in concentration, is observed.

Charge can facilitate initial droplet formation by reducing the required critical supersaturation, and stabilize small droplets against evaporation. Both processes will act to increase the abundance of small droplets, as observed. The droplet charge and local humidity are therefore critical in determining what occurs.

In our laboratory experiments using acoustically levitated droplets, a single ionizer of the same model was able to generate Rayleigh disintegrations in droplets of ~100 μm size [29]. Such an "electrospray" approach to charging can yield charge levels up to a few times less than the Rayleigh limit [28,30]. In the fog experiment, the four emitters provided –2 nA, or 1.4×10^{10} negative ions s^{-1}. For a cylindrical region of unit area in the 3 m between emitters and detector, the additional negative ion generation would be about 5×10^9 ions m^{-3} s^{-1}, assuming uniform ion distribution with no wind removal or vertical electrical migration, which is typically smaller than turbulent dispersion scales (Table I). In calm, foggy conditions the artificial negative ion generation will therefore exceed the natural ion production rate [31,25] by ~500. Equally partitioned across 100 droplets cm^{-3}, this volumetric charge generation rate is equivalent to ~3000 e min^{-1} per droplet. (The measurements of Fig. 4 were determined 5 min after the emitters were switched on and Fig. 3(b) demonstrates

TABLE I. Summary data before and during fog circumstances.

Circumstances	Mean horizontal wind speed U (m s^{-1})	Horizontal wind standard deviation σ_u (m s^{-1})	Vertical wind standard deviation σ_w (m s^{-1})	Mean PG (V m^{-1})	Switching cycles	Detrended mean PG (V m^{-1})		
						Charge emitter on	Charge emitter off	t-test p value
Prefog	4.03	2.40	0.49	46.1	115	−0.25	0.24	$<10^{-5}$
Fog period	0.54	0.27	0.06	115.6	29	−0.45	0.51	$<10^{-5}$

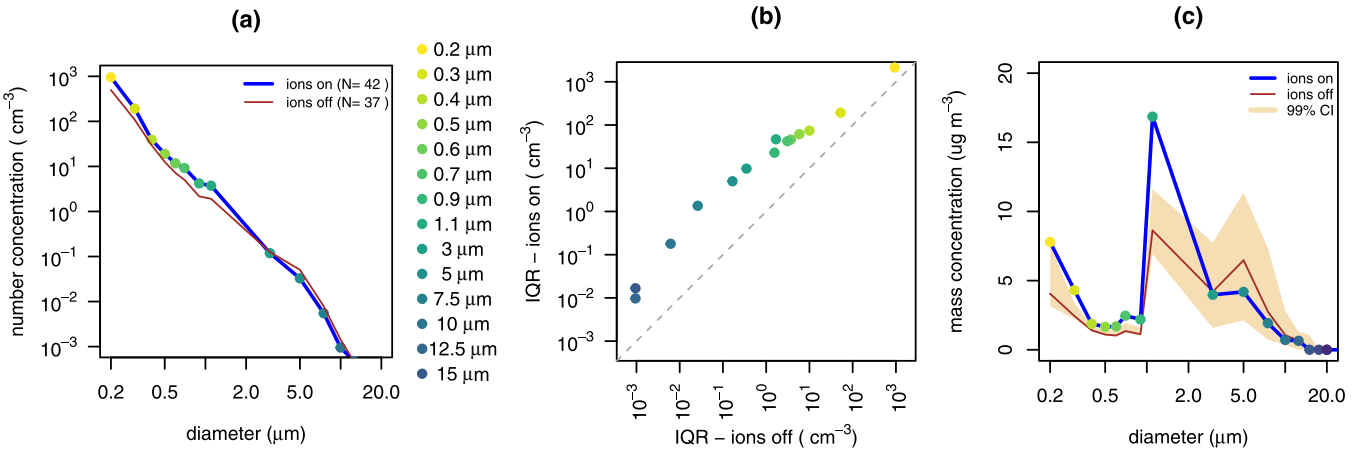

FIG. 4. Comparisons of droplet size distributions from LOAC scans during fog conditions, with emitters on and off. (a) Median droplet number concentration by diameter, colored by bin size. (b) Interquartile ranges (IQR) of the droplet concentrations by size during the emitter on and off periods, plotted against each other [colors show bin sizes, as for (a)]. (c) Median mass concentration by size bin, with 99% confidence interval (CI) on the median. (Concentrations are medians from the inner 5 min of the emitters on and off times: confidence ranges for the emitters off condition medians found by bootstrapping).

increased negative charge in the experimental volume). An abundance of negatively charged droplets, with lengthened evaporation times, or charged aerosols on which droplets can more readily form, is therefore likely.

V. CONCLUSION

Introducing ions influences natural droplet behavior, with an increase in droplet mass concentrations for micron size droplets observed after negative charge was emitted. This illustrates a possible route for weather modification, based on droplet physics rather than chemical materials, and supports a physical link between ionization and cloud behavior. It also suggests a method to be investigated further to displace aerosol mass, for example, of pathogens, towards larger sizes, ultimately facilitating gravitational removal.

ACKNOWLEDGMENT

This work was funded by the UAE Rain Enhancement Programme's project "Electrical aspects of rainfall generation." Data are available at [32].

[1] B. J. Mason, *The Physics of Clouds* (Oxford University Press, Oxford, 1971).

[2] W. Thomson, On the mutual attraction or repulsion between two electrified spherical conductors, in *Reprint of Papers on Electrostatics and Magnetism* (Cambridge University Press, Cambridge, 2011), pp. 86–97 (paper was first published in 1884).

[3] S. Banerjee, T. Peters, N. Brown, and Y. Song, Exact closed-form and asymptotic expressions for the electrostatic force between two conducting spheres, Proc. R. Soc. A **477**, 2246 (2021).

[4] J. Lekner, Electrostatics of two charged conducting spheres, Proc. R. Soc. A **468**, 2829 (2012).

[5] J. W. Strutt, The influence of electricity on colliding water drops, Proc. R. Soc. London **28**, 405 (1879).

[6] A. Khain, V. Arkhipov, M. Pinsky, Y. Feldman, and Y. Ryabov, Rain enhancement and fog elimination by seeding with charged droplets. Part I: Theory and numerical simulations, J. Appl. Meteorol. **43**, 1513 (2004).

[7] N. N. Klimin, V. Y. Rivkind, and V. A. Pachin, Collision efficiency calculation model as a software tool for microphysics of electrified clouds, Meteorol. Atmos. Phys. **53**, 111 (1994).

[8] S. E. Law, Agricultural electrostatic spray application: A review of significant research and development during the 20th century, J. Electrost. **51–52**, 25 (2001).

[9] J. L. Cadnum, A. L. Jencson, S. H. Livingston, D. F. Li, S. N. Redmond, B. Pearlmutter, B. M. Wilson, and C. J. Donskey, Evaluation of an electrostatic spray disinfectant technology for rapid decontamination of portable equipment and large open areas in the era of SARS-CoV-2, Am. J. Infect. Control **48**, P951 (2020).

[10] J. W. Tang, L. C. Marr, Y. Li, and S. J. Dancer, Covid-19 has redefined airborne transmission, BMJ **373**, n913 (2021).

[11] R. G. Harrison, K. A. Nicoll, and M. H. P. Ambaum, On the microphysical effects of observed cloud edge charging, Q. J. R. Meteorol. Soc. **141**, 2690 (2015).

[12] R. G. Harrison, K. A. Nicoll, M. H. P. Ambaum, G. J. Marlton, K. L. Aplin, and M. Lockwood, Precipitation Modification by Ionization, Phys. Rev. Lett. **124**, 198701 (2020).

[13] K. A. Nicoll and R. G. Harrison, Stratiform cloud electrification: Comparison of theory with multiple in-cloud measurements, Q. J. R. Meteorol. Soc. **142**, 2679 (2016).

[14] R. J. Pilié, E. J. Mack, W. C. Kocmond, W. J. Eadie, and C. W. Rogers, The life cycle of valley fog. Part II:

Fog microphysics, J. Appl. Meteorol. and Climatol. **14**, 364 (1975).
[15] H. R. Pruppacher, J. D. Klett, and P. K. Wang, Microphysics of clouds and precipitation, Aerosol Sci. Technol. **28**, 381 (1998).
[16] H. Zhang, D. Li, L. Xie, and Y. Xiao, Documentary research of human respiratory droplet characteristics, Procedia Eng. **121**, 1365 (2015).
[17] M. H. P. Ambaum, *Thermal Physics of the Atmosphere* (Elsevier, Amsterdam, 2021).
[18] R. G. Harrison and M. H. P. Ambaum, Enhancement of cloud formation by droplet charging, Proc. R. Soc. A **464**, 2561 (2008).
[19] D. Duft, T. Achtzehn, R. Müller, B. A. Huber, and T. Leisner, Coulomb fission: Rayleigh jets from levitated microdroplets, Nature (London) **421**, 128 (2003).
[20] W. H. Press, B. P. Flannery, S. A. Teukolsky, and W. T. Vetterling, Numerical recipes in PASCAL—the art of scientific computing, Math. Comput. **56**, 396 (1991).
[21] J. Lu, H. Nordsiek, E. W. Saw, and R. A. Shaw, Clustering of Charged Inertial Particles in Turbulence, Phys. Rev. Lett. **104**, 184505 (2010).
[22] Y. Yao and J. Capecelatro, Competition between drag and Coulomb interactions in turbulent particle-laden flows using a coupled-fluid-Ewald-summation based approach, Phys. Rev. Fluids **3**, 034301 (2018).
[23] M. H. P. Ambaum, T. Auerswald, R. Eaves, and R. G. Harrison, Enhanced attraction between drops carrying fluctuating charge distributions, Proc. R. Soc. A **478**, 20210714 (2022).
[24] R. Gunn, Diffusion charging of atmospheric droplets by ions, and the resulting combination coefficients, J. Meteorol. **11**, 339 (1954).
[25] R. G. Harrison and K. S. Carslaw, Ion-aerosol-cloud processes in the lower atmosphere, Rev. Geophys. **41**, 1012 (2003).
[26] J. B. Renard, F. Dulac, G. Berthet, T. Lurton, D. Vignelles, F. Jégou, T. Tonnelier, M. Jeannot, B. Couté, R. Akiki, N. Verdier, M. Mallet, F. Gensdarmes, P. Charpentier, S. Mesmin, V. Duverger, J. C. Dupont, T. Elias, V. Crenn, J. Sciare *et al.*, LOAC: A small aerosol optical counter/sizer for ground-based and balloon measurements of the size distribution and nature of atmospheric particles—Part 1: Principle of measurements and instrument evaluation, Atmos. Meas. Tech. **9**, 1721 (2016).
[27] See Supplemental Material at http://link.aps.org/supplemental/10.1103/PhysRevResearch.4.L022050 for additional plots and experimental details.
[28] J. B. Renard, S. N. Tripathi, M. Michael, A. Rawal, G. Berthet, M. Fullekrug, R. G. Harrison, C. Robert, M. Tagger, and B. Gaubicher, *In situ* detection of electrified aerosols in the upper troposphere and stratosphere, Atmos. Chem. Phys. **13**, 11187 (2013).
[29] M. W. Airey, R. G. Harrison, K. L. Aplin, and C. Pfrang, Effects of ionisation on cloud behaviour in planetary atmospheres, in Geophysical Research Abstracts (2021), https://doi.org/10.5194/egusphere-egu21-13639.
[30] J. P. Borra, Review on water electro-sprays and applications of charged drops with focus on the corona-assisted cone-jet mode for high efficiency air filtration by wet electro-scrubbing of aerosols, J. Aerosol Sci. **125**, 208 (2018).
[31] J. A. Chalmers, *Atmospheric Electricity* (Pergamon, Oxford, 1967).
[32] https://doi.org/10.17864/1947.334.